The effect of annealing on photoluminescence from defects in ammonothermal GaN

M. A. Reshchikov,[a] D. O. Demchenko,[a] D. Ye,[a] O. Andrieiev,[a] M. Vorobiov,[a] K. Grabianska,[b] M. Zajac,[b] P. Nita,[b] M. Iwinska,[b] M. Bockowski,[b] B. McEwen,[c] and F. Shahedipour-Sandvik[c]

[a] *Department of Physics, Virginia Commonwealth University, Richmond, VA 23220, USA*

[b] *Institute of High Pressure Physics, Polish Academy of Sciences, Sokolowska 29/37, Warsaw 01-142, Poland*

[c] *College of Nanoscale Science and Engineering, SUNY Polytechnic Institute, Albany NY 12203, USA*

Abstract

Ammonothermal GaN samples with the concentration of free electrons of 10^{18} and 10^{19} cm^{-3} were annealed in a wide range of temperatures (T_{ann} = 300-1400 °C) under atmospheric N_2 pressure and under ultra-high N_2 pressure conditions to avoid the GaN decomposition. Photoluminescence (PL) studies reveal the YL2 band with a maximum at 2.3 eV before annealing and two new PL bands after annealing at T_{ann} > 600 °C: the OL3 band with a maximum at 2.1 eV and the RL4 band with a maximum at 1.6-1.7 eV. The ammonothermal GaN samples have high concentrations of complexes containing gallium vacancy (V_{Ga}), hydrogen, and oxygen. The first-principles calculations suggest the V_{Ga}-$3H_i$ complex is the origin of the YL2 band, while the V_{Ga}-$3O_N$ complex is responsible for the RL4 band.

I. INTRODUCTION

Ammonothermal growth is a promising method for obtaining high-quality bulk GaN crystals. The crystals demonstrate outstanding structural properties, very low density of threading dislocations, yet contain a high concentration of point defects.[1] Point defects in GaN are still not well understood, and photoluminescence (PL) is one of the major tools for their study.[2,3] In addition to high concentrations of hydrogen and oxygen,[1] GaN grown by ammonothermal method (Am-GaN) contains high concentrations of gallium vacancies (V_{Ga}), at least 10^{18} cm^{-3}, as estimated from the positron annihilation spectroscopy and Fourier transform infrared spectroscopy. [4,5,6,7,8,9] Moreover, according to these studies, the V_{Ga} forms complexes with H and O. On the other hand, first-principles calculations using hybrid density functional theory predict that complexes containing V_{Ga}, H, and O, such as V_{Ga}-H, V_{Ga}-2H, V_{Ga}-O_N-H, V_{Ga}-3H, and V_{Ga}-O_N-2H, have low formation energy and may be responsible for several PL bands in GaN.[10]

Recently we reported [11] that the low-temperature PL spectrum from basic ammonothermal GaN contains three defect PL bands: the Mg-related ultraviolet luminescence (UVL) band with the zero-phonon line (ZPL) at 3.27 eV, the Zn-related blue luminescence (BL1) band with a maximum at 2.9 eV, and a new yellow luminescence (YL2) band with a maximum at 2.3 eV. An unusual property of the YL2 band is a large shift (up to ~0.1 eV) with increasing excitation intensity in steady-state PL (SSPL) experiments or with a time delay after a laser pulse in time-resolved PL (TRPL) studies. The shifts were preliminarily explained by the donor-acceptor pair (DAP) nature of transitions responsible for the YL2 band.

In this work, we present the results of first-principles calculations for the V_{Ga}-containing defects and detailed studies of PL from Am-GaN samples after annealing them in a wide range of temperatures (from 300 to 1400 °C).

II. METHODS

A. Calculations

Theoretical calculations were performed using the Heyd-Scuseria-Ernzerhof (HSE) hybrid functional.[12] The HSE functional was tuned to fulfill the generalized Koopmans condition for the V_{Ga} in GaN (fraction of exact exchange is 0.25, the range separation parameter is 0.161 Å^{-1}).[13] Calculations were performed in 128-atom hexagonal supercells at the **Γ**-point, with plane-wave energy cutoffs of 500 eV. All defect atomic structures were relaxed within HSE to minimize forces to 0.05 eV/Å or less. Spurious electrostatic interactions in calculated total energies were corrected using the Freysoldt-Neugebauer-Van de Walle approach.[14,15] Defect formation energies were calculated following the procedure outlined in Ref. 16. The formation energy of a defect D in a charge state q is calculated as

$$E_f(D^q) = E_{tot}(D^q) - E_{tot}(\text{bulk}) - \sum_i n_i\mu_i + q(E_{VBM} + E_F) + \Delta_q, \quad (1)$$

where $E_{tot}(D^q)$ is the total energy if the supercell with the defect D and $E_{tot}(\text{bulk})$ is the total energy of the pristine supercell. The numbers of atoms of type i that are removed from or added to the supercell is n_i, and μ_i is the elemental chemical potential of the i-th atom. E_{VBM}, E_F, and Δ_q are the energy of the valence band maximum, the Fermi energy, and the correction for the spurious electrostatic interactions. Adiabatic potentials used to plot the configuration coordinate diagrams were obtained by fitting into HSE computed total energies using harmonic approximation and mapping the atomic displacements ΔR_i onto the configuration coordinate Q as $\Delta Q^2 = \sum_{i,x,y,z} m_i \Delta R_i^2$, where m_i are the atom masses. Elemental chemical potentials used in defect formation energy calculations were obtained from the total energies of the GaN growth competing phases. In a nitrogen-rich growth regime, the chemical potential of nitrogen is set to $\mu_N(N_2)$, while that of

gallium is set to $\mu_{\mathrm{Ga}}(\mathrm{Ga\ metal}) + \Delta H_f(\mathrm{GaN})$, where $\Delta H_f(\mathrm{GaN})$ is the formation enthalpy of GaN (computed to be -1.2 eV). The chemical potential of oxygen is assumed to be limited by the formation of gallium oxide Ga_2O_3, and the formation of ammonia determines the chemical potential of hydrogen. Note that the defect transition levels and optical transition energies, which are the focus of this work, are independent of the choice of the chemical potentials.

B. Samples and annealing details

Unintentionally doped *c*-plane GaN wafers with a diameter of 1 inch and thickness of 370 μm were prepared from ammonothermally-grown crystals. The crystals were grown at temperatures 500-600 °C and pressure 0.3-0.4 GPa under a basic environment. The details of ammonothermal technology are described elsewhere.[1,17,18,19] Two types of samples were studied: the high-transparency wafers (Am-*n*-GaN samples) and the high electron concentration substrates (Am-n^+-GaN samples); see Ref. 1 for a detailed description. According to secondary-ion mass spectrometry (SIMS) studies, the main impurities in Am-*n*-GaN samples are H, O (both ~10^{18} cm^{-3}), Si, C (~10^{17} cm^{-3}), Zn, Mg (mid-10^{16} cm^{-3}).[1] The concentration of H and O in Am-n^+-GaN samples is an order of magnitude higher. The free-electron concentration in Am-*n*-GaN samples and Am-n^+-GaN samples is about 1×10^{18} and 1×10^{19} cm^{-3}, respectively.[1,11] The high concentrations of free electrons in undoped GaN grown by ammonothermal method (~10^{19} cm^{-3}) is related to high concentration of oxygen originating from ammonothermal environment (the O_N defect is a shallow donor in GaN). In Am-*n*-GaN samples, the concentration of oxygen has been reduced by introducing an oxygen getter into the crystal growth system.[1]

The samples were cut into smaller pieces and annealed in N_2 ambient without any protective layer. In the first type of annealing, a single-zone quartz tube furnace was used. The annealing was conducted at atmospheric pressure for one hour and temperatures, T_{ann}, from 300 to 1100 °C. In

the second type of annealing, we employed ultra-high-pressure-annealing (UHPA).[20] The samples were annealed for one hour at nitrogen pressure of 1 GPa and T_{ann} = 1000 – 1400 °C.

C. Experimental details

The SSPL and TRPL were excited with HeCd and nitrogen lasers, respectively. The as-measured PL spectra were corrected for the measurement system's spectral response, and PL intensity was additionally multiplied by λ^3, where λ is the light wavelength, to present the PL spectra in units proportional to the number of emitted photons as a function of photon energy.[21] The absolute quantum efficiency, η, for each PL band was obtained by comparing the integrated PL intensity with that from calibrated GaN samples.[3,21,22] Other details of PL experiments can be found elsewhere.[3,21]

III. THEORY

Based on the SIMS data available for ammonothermal GaN, we performed calculations of energetics and optical properties of complexes containing V_{Ga}, H, and O. In terms of their optical properties, the defect complexes fall into two categories. First, the deep donors for which nonradiative hole capture occurs with nearly no potential barrier, with subsequent radiative recombination. Second, the deep multi-charged defects, which are negatively charged in *n*-type GaN, and for which a large potential barrier hinders the nonradiative hole capture. The existence of excited states due to multiple spin configurations suggests that these defects are likely nonradiative Shockley-Read-Hall recombination centers.

An example of the defect complex from the first category is presented in Fig. 1, where the configuration coordinate diagram for the V_{Ga}-$3H_i$ complex is shown. This complex is a deep donor with the 0/+ transition level at 0.72 eV above the valence band maximum (VBM). In *n*-type

samples, this defect is in the neutral charge state (lower potential in Fig. 1), for which the calculated formation energy is relatively low (0.4 eV). A photogenerated electron-hole pair raises the system's energy by E_g = 3.5 eV (upper potential in Fig. 1). The complex captures the hole nonradiatively with no potential barrier via the multi-phonon emission process, as shown with a dashed arrow in Fig. 1, converting the complex into positively charged. The nonradiative transition from the positive charge state to the neutral ground state is unlikely because of a large potential barrier for this process, about 1.2 eV. The transition is likely to be radiative, with an expected ZPL (E_0) at 2.78 eV and a PL maximum ($\hbar$) at 2.13 eV, placing the PL band in the yellow part of the spectrum. These parameters are close to those obtained for the YL2 band, i.e., PL maximum at 2.3 eV and ZPL at ~2.9 eV.[11]

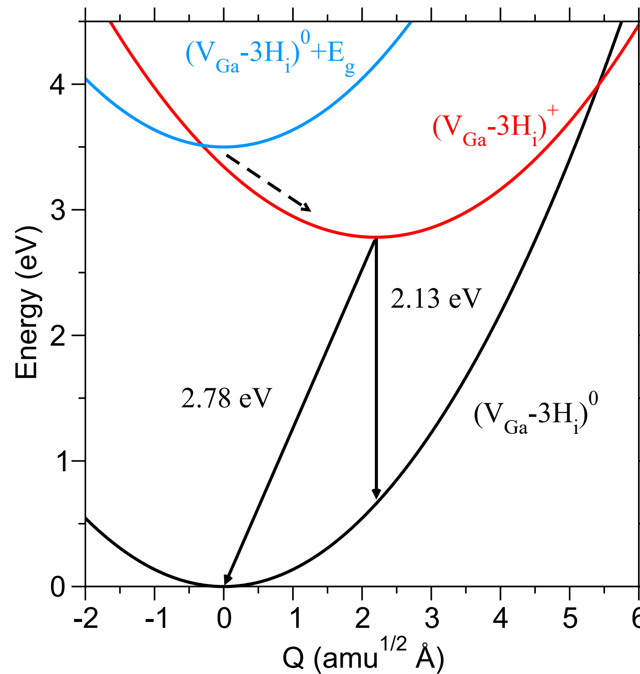

Fig. 1. (Color online) Configuration coordinate diagram describing the 0/+ transition of the V_{Ga}-$3H_i$ complex. In the ground state, the defect is neutral. A photogenerated hole is captured (dashed arrow) by the defect, with subsequent radiative transitions calculated to have the PL maximum at 2.13 eV and the ZPL at 2.78 eV.

The V_{Ga} complexes containing three donors (H_i or O_N) exhibit similar properties, i.e., they all are deep donors with somewhat varying values of transition energies (summarized in Fig. 2). Namely, $\hbar$ = 1.92 eV and E_0 = 2.57 eV for the V_{Ga}-O_N-$2H_i$ complex, $\hbar$ = 1.79 eV and E_0 = 2.40 eV for the V_{Ga}-$2O_N$-H_i complex, and $\hbar$ = 1.67 eV and E_0 = 2.28 eV for the V_{Ga}-$3O_N$ complex. Their computed formation energies are also similar and low (summarized in Table I), around 0.4-0.5 eV in the neutral charge state (in *n*-type GaN), except for the V_{Ga}-$3O_N$ complex, which is somewhat higher in energy at 1.1 eV.

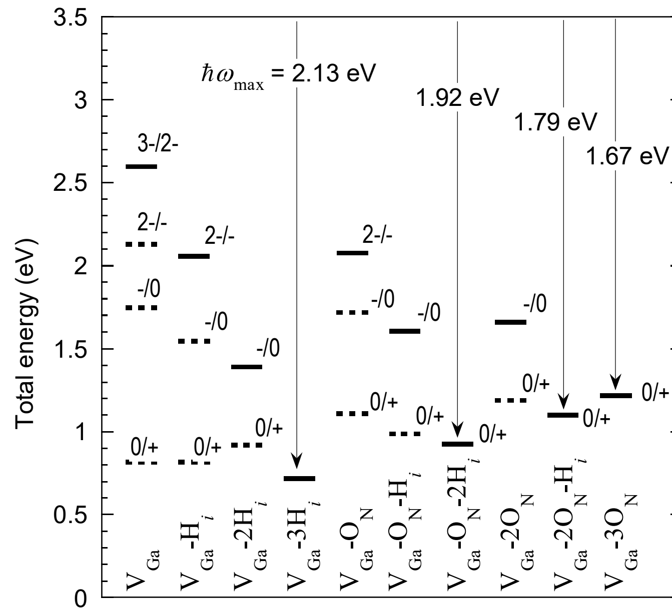

Fig. 2. (Color online) Charge transition levels of defect complexes containing V_{Ga}, H_i, and O_N in the bandgap of GaN. The transition levels that participate in electron-hole recombination in conductive *n*-type GaN are shown with solid bars. The transition levels shown with dashed bars are not active in conductive *n*-type GaN and cannot be studied by PL. The ZPLs for PL bands of optically active defects are shown with vertical arrows. The indicated energies for radiative transitions correspond to $\hbar$ (not the ZPL).

A typical configuration coordinate diagram for a defect from the second category is shown in Fig. 3, using the V_{Ga}-$2H_i$ complex as an example. These complexes exhibit both deep donor and acceptor transition levels. In *n*-type GaN, these defects are negatively charged and could be expected to attract a photogenerated hole. However, nonradiative hole capture by this defect is inefficient due to a large potential barrier for this process. For example, the barrier for the hole capture by the negatively charged V_{Ga}-$2H_i$ complex is 1.45 eV. Therefore, a photogenerated hole can be captured radiatively, i.e., cause infrared PL (dashed arrow in Fig. 3). Then second radiative transition would occur, producing a PL band with $\hbar$ = 1.82 eV and E_0 = 2.11 eV. However, in *n*-type samples, where holes are minority carriers, the first transition has a very low probability because this relatively slow process (the radiative lifetimes are usually on the microseconds scale) competes with the fast nonradiative hole capture by other defects and excitonic emission. Thus, complexes of the second category are not expected to contribute to PL.

A number of the V_{Ga} complexes considered here exhibit such properties: V_{Ga}-H_i, V_{Ga}-O_N, V_{Ga}-O_N-H_i, V_{Ga}-$2O_N$, as well as transition via the 3−/2− state of the isolated V_{Ga}. These defects also have somewhat higher formation energy than the deep donors discussed above, by 1-2 eV (Table I).

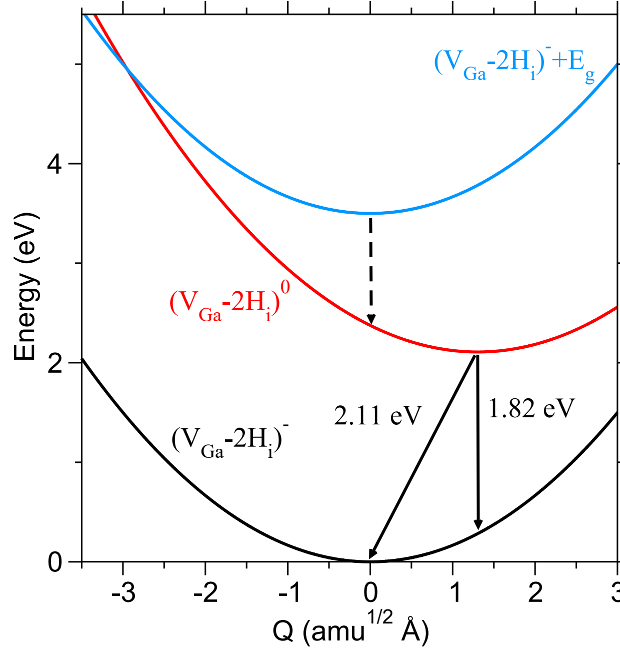

Fig. 3. (Color online) Configuration coordinate diagram describing the −/0 transition of the V_{Ga}-$2H_i$ complex. In the ground state, the defect is negatively charged. The potential barrier for the nonradiative capture of the photogenerated hole is 1.45 eV. Radiative capture of the hole by the defect (the dashed arrow) can transfer the defect into a neutral charge state. The subsequent radiative transitions have the PL maximum at 1.82 eV and the ZPL at 2.11 eV. In *n*-type GaN, such a process is very inefficient (see the text).

In addition, the excited states, not accounted for in our calculations, may drastically increase the efficiency of the Shockley-Read-Hall electron-hole recombination via multi-charged defects. Alkauskas *et al.*[23] have shown that instead of the slow radiative capture, the hole can be quickly captured nonradiatively by an excited state of the defect, after which a series of nonradiative transitions to the ground state occurs (the intra-defect relaxation). As an example, these authors consider the V_{Ga}-O_N complex with the calculated 2−/− level at 2.17 eV above the VBM (2.08 eV in this work). They show that while the nonradiative hole capture at the 2−/− level is negligibly slow, a photogenerated hole can be efficiently captured by an excited state of this defect located at 1.15 eV above the VBM. Overall, accounting for the excited states increases the Shockley-Read-

Hall recombination rate of a multi-charged defect by several orders of magnitude. Thus, the excited states can drastically increase the nonradiative recombination efficiency via defects from the second category.

All transition levels for the V_{Ga} and its complexes with H_i and O_N are summarized in Table I. The removal energies are given with respect to dissociating a complex into a positively charged donor (H^+_i or O^+_N) and remaining complex constituents in *n*-type conditions. For example, the removal energy of the neutral $(V_{Ga}\text{-}3H_i)^0$ is the difference of formation energies of the constituents H_i^+ plus $(V_{Ga}\text{-}2H_i)^-$ and the formation energy of the $(V_{Ga}\text{-}3H_i)^0$ complex.

Table I. HSE calculated formation energies, removal energies, and thermodynamic transition levels $\varepsilon(q_1/q_2)$ of the V_{Ga}-containing complexes with respect to the VBM. Formation energies of all defects are given assuming the nitrogen-rich growth regime for *n*-type GaN samples, i.e., the Fermi energy at the conduction band minimum.

Defect	q_1/q_2	Transition energy (eV)	Formation energy (eV)	Removal energy (eV)
V_{Ga}	0/+	0.82		
	–/0	1.75		
	2–/–	2.13		
	3–/2–	2.60	2.49	
V_{Ga}-H_i	0/+	0.82		
	–/0	1.55		
	2–/–	2.06	1.00	4.51
V_{Ga}-$2H_i$	0/+	0.92		
	–/0	1.39	0.33	3.71
V_{Ga}-$3H_i$	0/+	0.72	0.39	2.97
V_{Ga}-$4H_i$	0/+	>3.4 (shallow donor)	1.41	4.05
V_{Ga}-O_N	0/+	1.11		
	–/0	1.72		
	2–/–	2.08	1.64	3.60
V_{Ga}-O_N-H_i	0/+	0.99		
	–/0	1.61	0.66	3.71
V_{Ga}-O_N-$2H_i$	0/+	0.93	0.47	3.22
V_{Ga}-$2O_N$	0/+	1.19		
	–/0	1.66	1.15	3.22
V_{Ga}-$2O_N$-H_i	0/+	1.10	0.72	3.46
V_{Ga}-$3O_N$	0/+	1.22	1.10	2.79
V_{Ga}-$3O_N$-H_i	0/+	>3.4 (shallow donor)	0.73	3.00

In terms of the positions of the transition levels in the bandgap of GaN, our results are similar to those obtained by Lyons *et al.*,[10] which showed that these complexes exhibit similar values for the donor and acceptor levels. When the V_{Ga} forms a complex with hydrogen, with the addition of each H atom, a nitrogen dangling bond is passivated, removing a transition level from the bandgap. A fully hydrogen passivated gallium vacancy, i.e., the V_{Ga}-$4H_i$ complex, acts as a shallow donor. The addition of oxygen, i.e., substituting nitrogen atoms, slightly raises the transition levels. Overall, only the deep donor complexes with a single 0/+ transition level in the

bandgap are expected to produce measurable PL at photon energies above 1.5 eV. The transition energies are redshifted with the addition of oxygen due to the rising transition level in the bandgap (Fig. 2). The remaining V_{Ga} complexes are not expected to cause a significant PL in *n*-type GaN.

Hydrogen, at least in *p*-type and high-resistivity *n*-type GaN, is a volatile element, which usually forms relatively weakly bound complexes with defects in GaN.[24,25] Therefore one may expect that annealing of ammonothermal GaN samples would lead to the decreasing PL intensity from the V_{Ga}-containing donor complexes due to removal of hydrogen and converting, for example, V_{Ga}-3H_i into V_{Ga}-2H_i, and V_{Ga}-O_N-2H_i into V_{Ga}-O_N-H_i, etc. At the same time, removing a hydrogen atom from the V_{Ga}-3O_N-H_i, which is a shallow donor with a relatively low formation energy of about 0.7 eV in *n*-type GaN, can lead to the formation of the radiative V_{Ga}-3O_N complex. The latter is predicted to produce a PL band with the maximum at 1.67 eV and ZPL at 2.28 eV.

IV. EXPERIMENTAL RESULTS

A. Photoluminescence from GaN before annealing

Figure 4 shows typical low-temperature PL spectra from Am-*n*-GaN and Am-n^+-GaN samples before annealing (the reference samples).[11] The near-band-edge (NBE) emission band is relatively weak because it competes with PL from point defects abundant in these samples. In particular, Mg and Zn impurities, found in ammonothermal GaN with concentrations of 10^{16}-10^{17} cm^{-3}, are responsible for the strong UVL band with the first peak at 3.27 eV followed by LO phonon replicas and the BL1 band with a maximum at about 2.9 eV.[11] A broad PL band with a maximum at ~2.3 eV, labeled YL2, is presumably caused by a V_{Ga}-containing defect. The characteristic features of the YL2 band are a nonexponential decay after a laser pulse and a significant blue shift with increasing excitation intensity in SSPL or a red shift after a laser pulse in TRPL (by up to 0.1 eV).[11]

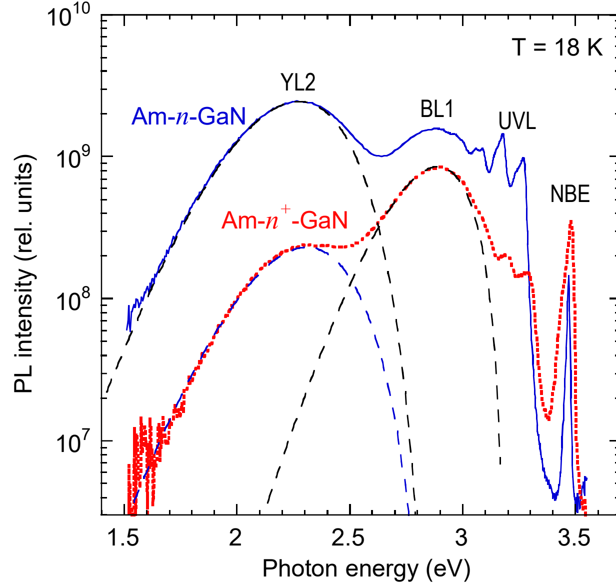

Fig. 4. (Color online) Low-temperature PL spectra from Am-n-GaN and Am-n^+-GaN samples before annealing. The dashed lines are calculated using Eq. (2) with parameters given in Table II.

Broad PL bands from defects in GaN have reproducible shapes that can be fitted with the following expression obtained in a one-dimensional configuration coordinate model.[26]

$$I^{PL}(\hbar \quad \hbar \quad \left[-2S_e \left(\sqrt{\frac{E_0^* - \hbar}{E_0^* - \hbar}} \quad 1 \right)^2 \right]. \tag{2}$$

Here, S_e is the Huang-Rhys factor in the excited state of the defect, $E_0^* = E_0 + 0.5\hbar$, E_0 is the ZPL energy, $\hbar$ is the energy of the effective phonon mode in the excited state, $\hbar$ and $\hbar$ are the photon energy and position of the PL band maximum, respectively. The Δ is a small shift of the PL band maximum due to sample-dependent reasons. For example, the Am-n^+-GaN samples are degenerate, with the Fermi level in the conduction band, so that all PL bands are usually shifted

to higher energies by about Δ = 0.03 eV.[11] Table II presents the parameters S_e, $\hbar\Omega$, and E_0^*, which can be used to reproduce shapes of broad PL bands in ammonothermal GaN by using Eq. (2). The uncertainty of the found parameters S_e and E_0^* is relatively high for the broad bands (except for the BL1) because no ZPL is observed and the PL bands overlap. For example, a similar shape of the YL2 band (with a slightly expanded high-energy side) can be obtained by using E_0^* = 3.0 and S_e = 10.5. In this work, we will use the parameters from Table II with the only purpose to reproduce shapes of broad PL bands in the studied samples and deconvolute PL spectra where several PL bands overlap.

Table II. Defect-related PL bands in ammonothermal GaN, parameters in Eq. (2) defining the bands' positions and shapes, and the expected charge transition levels above the top of the VBM (E_i).

PL band	Preliminary attribution	$\hbar\Omega$ (eV)	S_e	E_0^* (eV)	E_i (eV)
BL1	Zn_{Ga}	2.86	3.2	3.14	0.4
YL2	V_{Ga}-$3H_i$	2.3	7.3	2.86	~0.6
OL3	Unknown	2.09	13	2.8	~0.7
RL4	V_{Ga}-$3O_N$	1.6-1.7	9	2.26	~1.2

B. The effect of annealing

GaN samples were annealed in atmospheric pressure N_2 at temperatures between 300 and 1100 °C. The PL spectra at T = 18 K for selected annealing temperatures are shown in Fig. 5. The PL spectra up to T_{ann} = 400 °C were the same as in the reference samples (Fig. 4). At higher annealing temperatures, two new PL bands appeared: the orange luminescence (OL3) with a maximum at

2.1 eV and the red luminescence (RL4) at 1.6-1.7 eV. The shapes and positions of the broad bands are reproducible in samples annealed at different temperatures. With increasing T_{ann}, the new PL bands intensities increase and reach a maximum at $T_{ann} \approx 1000$ °C, where the RL4 band becomes the strongest PL band with quantum efficiency approaching unity. As a consequence, the intensities of other PL bands drop (Fig. 5b).

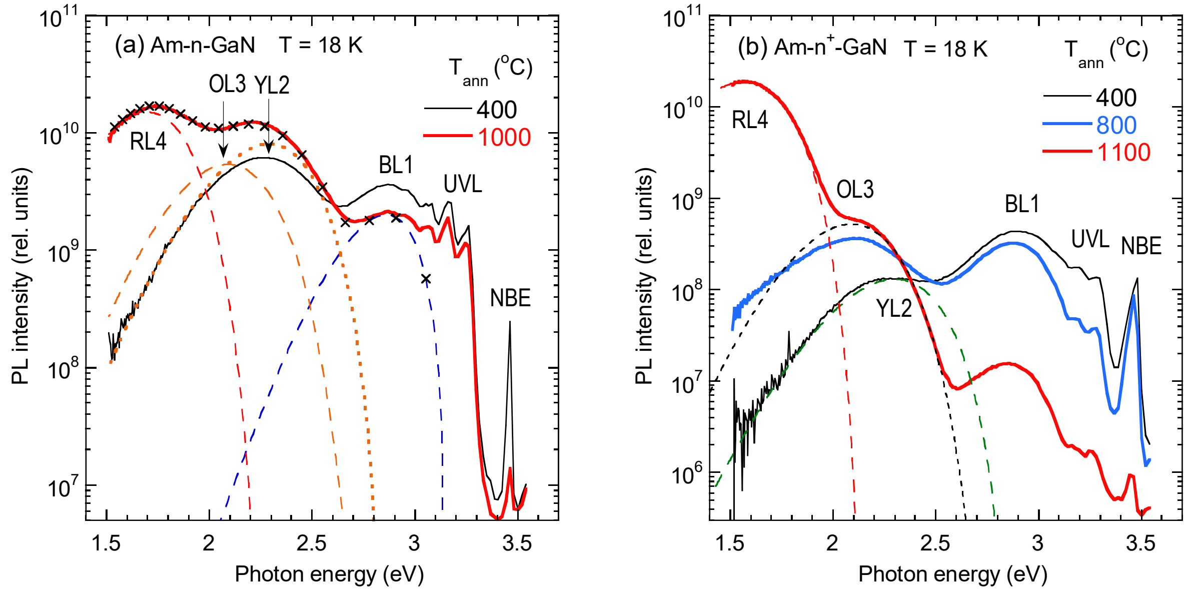

Fig. 5. (Color online) Low-temperature PL spectra from Am-*n*-GaN (a) and Am-n^+-GaN (b) annealed at selected T_{ann} under atmospheric pressure N_2. The dashed lines are calculated using Eq. (2) with parameters given in Table II.

Samples were also annealed at higher temperatures (T_{ann} = 1000, 1250, 1300, 1350, and 1400 °C) by the UHPA method. PL spectra at selected temperatures are shown in Fig. 6. At $T_{ann} > 1250$ °C the intensities of the YL2, OL3, and RL4 bands decrease, whereas the intensities of the BL1, UVL, and NBE bands simultaneously increase. After the deconvolution of the PL spectra, the PL quantum efficiencies for each PL band were obtained and plotted as a function of T_{ann} (Fig. 7). It should be kept in mind that different N_2 pressure could affect the concentrations of defects. However, we did not notice any substantial differences in PL intensities (more than the scatter due

to different samples and annealing repetitions) for samples annealed at atmospheric pressure and the UHPA at the same temperature (1000 °C).

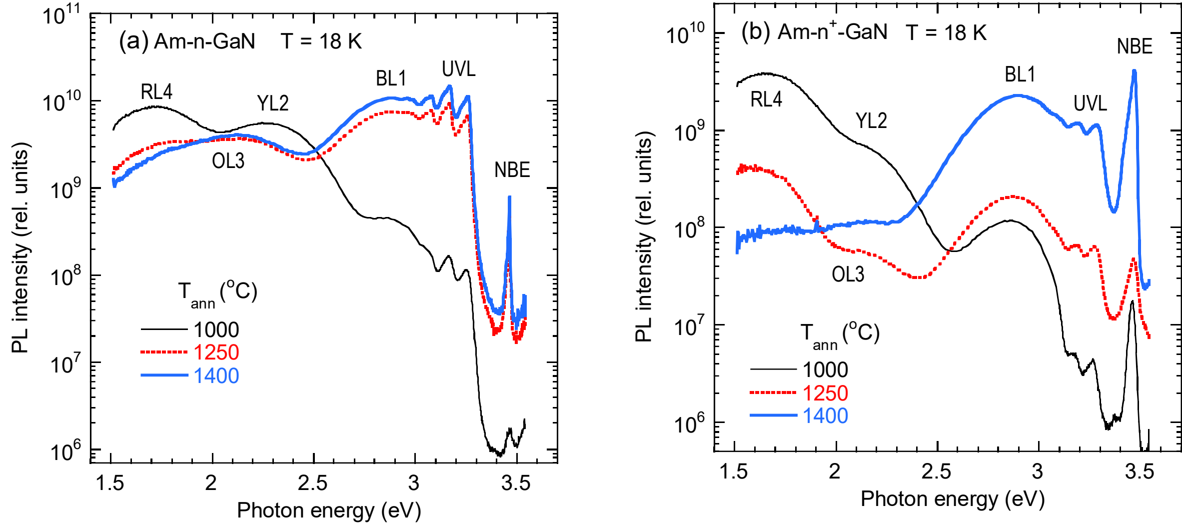

Fig. 6. (Color online) Low-temperature PL spectra from Am-*n*-GaN (a) and Am-n^+-GaN (b) annealed at selected T_{ann} under UHPA.

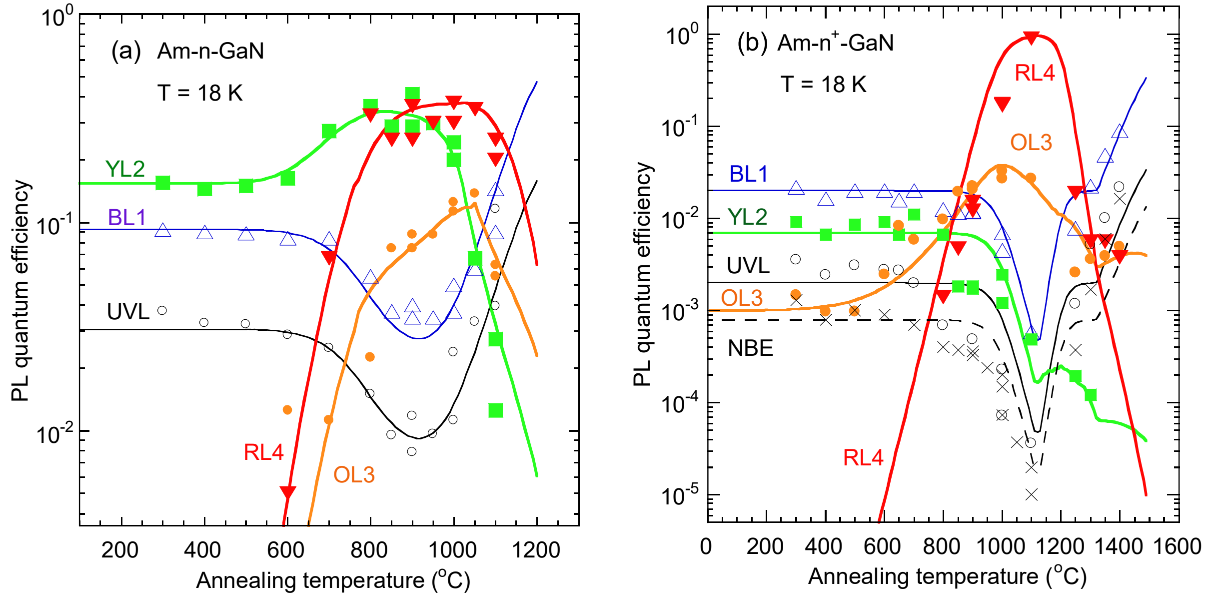

Fig. 7. (Color online) The dependences of the PL quantum efficiency on T_{ann} for PL bands in Am-*n*-GaN samples (a) and Am-n^+-GaN samples (b). The symbols are experimental data, and the lines are calculated using Eq. (4) with the $N_iC_{pi}(T_{\text{ann}})$ dependences shown in Fig. 11.

For samples with a moderate concentration of free electrons (Am-*n*-GaN), a sharp rise of the RL4 band is observed at $T_{ann} > 600$ °C. The quantum efficiency of the RL4 band is close to unity at 800-1000 °C, and it decreases at higher T_{ann} (Figs. 5a, 6a, and 7a). Simultaneously with the RL4 increase, the YL2 intensity slightly increases, and the OL3 band emerges. The intensities of the YL2, OL3, and RL4 bands decrease above 1000-1100 °C. For degenerate GaN with a high concentration of free electrons (Am-n^+-GaN), the RL4 band appears at $T_{ann} \approx 800$ °C, and at 1100 °C it becomes the strongest PL band with the quantum efficiency close to one (Figs. 5b and 7b). The YL2 efficiency decreases at $T_{ann} > 800$ °C, and it becomes weaker than the OL3 band. The RL4 and OL3 intensities start decreasing above 1100 °C.

Interestingly, the UVL, BL1, and NBE intensities decrease significantly at T_{ann} when the total quantum efficiency of other PL bands (RL4, OL3, and YL2) is close to one. This is the result of a competition for photogenerated holes between recombination channels in conductive *n*-type GaN (Sec. VA).[3] At higher T_{ann}, the RL4, OL3, and YL2 efficiencies drop, resulting in simultaneous emergence of the UVL, BL1, and NBE bands (Figs. 5-7). The very high quantum efficiency of the BL1 band in Am-*n*-GaN annealed at 1400 °C was also confirmed by the evolution of the PL spectrum with increasing measurement temperature T. The quenching of the BL1 band at $T > 200$ K in that sample resulted in the simultaneous increase of intensities of other PL bands by a factor of two, indicating that the quantum efficiency of the BL1 band before the quenching is about 0.5. While the OL3 and YL2 bands often overlap in PL spectra, the RL4 band could be well resolved at $T_{ann} = 1000$-1100 °C, which let us study it in more detail.

C. The RL4 band in ammonothermal GaN

The quantum efficiency of the RL4 band for several samples as a function of annealing temperature is replotted in the form of the Arrhenius plot in Fig. 8. In Am-*n*-GaN, the RL4 intensity

increases with the activation energy $E_A \approx 2$ eV above 600 °C. Its quantum efficiency is close to unity from 800 to 1100 °C. At higher temperatures, the RL4 intensity decreases. The RL4 band in Am-n^+-GaN appears at $T_{ann} \approx 800$ °C and increases with $E_A = 2.7$ eV. It reaches the quantum efficiency of unity at 1100 °C and decreases at higher T_{ann} with the activation energy of 3.2 eV.

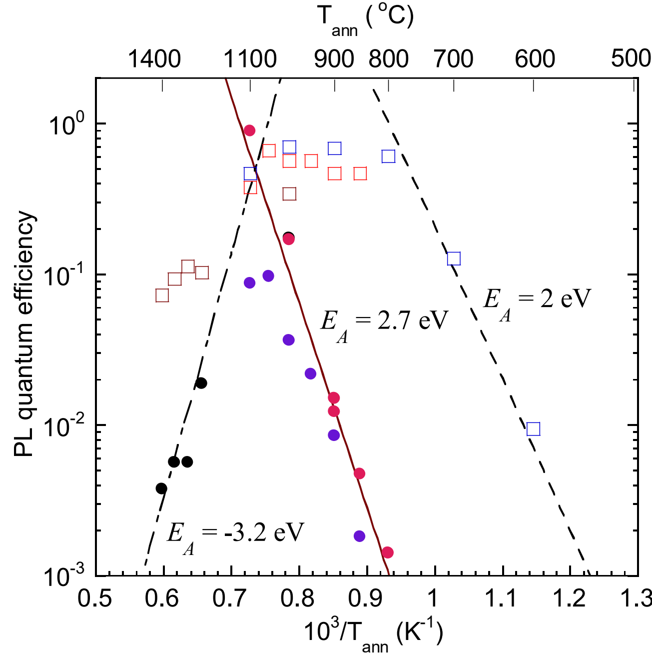

Fig. 8. (Color online) The dependences of the RL4 quantum efficiency on T_{ann} in Am-n-GaN samples (empty squares) and Am-n^+-GaN samples (solid circles) annealed under atmospheric pressure N_2 (T_{ann} = 600-1100 °C) and UHPA (T_{ann} = 1000-1400 °C). Different samples are shown with different symbol colors. The lines are calculated dependences of the form $\exp(-E_A/kT)$ with the parameter E_A indicated.

With increasing PL measurement temperature T, the quenching of the UVL, BL1, and YL2 bands was similar to that in the reference GaN samples.[11] The intensity of the RL4 band in the Am-n^+-GaN samples annealed at 1000-1100 °C remained unchanged up to T = 320 K. Because

PL bands broaden with T, we could not resolve the OL3 band at high T and study its quenching behavior.

D. Time-resolved photoluminescence

We studied TRPL for selected samples containing the YL2, OL3, and RL4 bands. Figure 9a shows low-temperature TRPL spectra at time delays from 10^{-8} to 10^{-4} s after a laser pulse for the Am-n^+-GaN sample annealed at 1000 °C. The spectra were deconvoluted using fixed shapes of the broad PL bands obtained with Eq. (2) and parameters from Table II. The BL1, YL2, OL3, and RL4 bands were resolved, and their peak intensities as a function of time delay are shown in the inset to Fig. 9b. Figure 9b shows the decay of the RL4 intensity (normalized at the limit of short times) for the Am-n^+-GaN sample annealed at 1000 and 1100 °C.

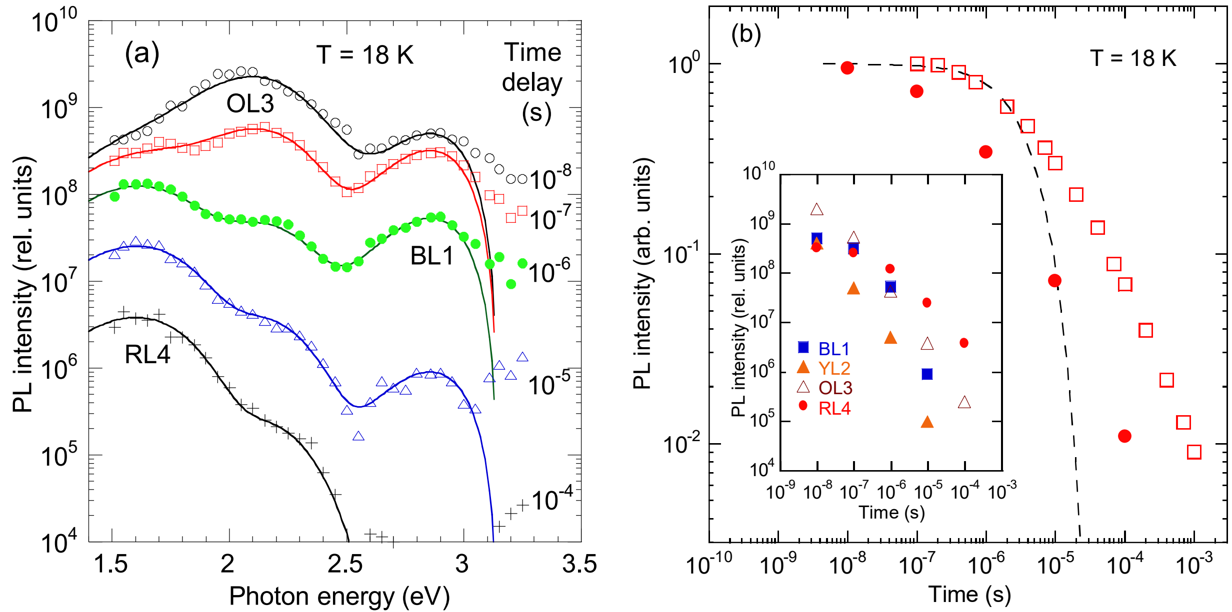

Fig. 9. (Color online) Time-resolved PL from Am-n^+-GaN annealed under atmospheric pressure N_2. (a) PL spectra at selected time delays after a laser pulse. The symbols show experimental data for a sample annealed at T_{ann} = 1000 °C. The lines are obtained by fitting the intensities of the broad PL bands with the fixed shapes defined by parameters in Table

II. (b) Normalized decay curve of the RL4 intensity after a laser pulse for a sample annealed at 1000 °C (filled circles) and 1100 °C (empty squares). The dashed curve is the exponential decay with $\tau = 2$ μs. The inset in (b) shows the time dependences for the broad bands obtained from deconvolution of the spectra shown in (a).

The decays of all the defect-related bands in the studied samples are nonexponential, yet the effective PL lifetime, τ^*, defined as time at which the $I^{PL}t(t)$ dependence has a maximum,[27] can be found. In conductive n-type GaN, $\tau^* = (nC_n)^{-1}$, where n is the concentration of free electrons and C_n is the electron-capture coefficient for a defect causing the PL. For the BL1 band in Am-n^+-GaN and Am-n-GaN samples, $\tau^* \approx 0.5$ and 4.5 μs, respectively, at $T = 20$ K before annealing.[11] However, the decays of the RL4 band appear to be sample-dependent and are not strictly exponential. The τ^* for the RL4 band in Am-n^+-GaN annealed at $T_{ann} = 1000$-1100 °C are in the ranges of 50-500 μs at $T = 18$ K and 10-120 μs at $T = 300$ K. The τ^* for the OL3 band in these samples is shorter by a factor of ~20. For Am-n-GaN sample annealed at $T_{ann} = 850$-1000 °C the τ^* for the RL4 band is 400-700 μs at room temperature. In all the cases, a long nonexponential tail extends to the milliseconds range. The TRPL spectra are consistent with the SSPL spectra, and the PL bands shapes are the same in both cases (described with parameters given in Table II). No significant shift of the RL4 and OL3 bands is noticed with time delay.

We conclude that the OL3 and RL4 bands are caused by electron transitions from the conduction band to the defect levels located at ~0.7 and ~1.2 eV, respectively, above the VBM. The long nonexponential tails in PL decays could be caused by local electric fields common for heavily doped semiconductors.[2] We exclude the possibility that the OL3 and RL4 bands are caused

by internal transitions (from an excited state to the ground state) because in that case the PL decays would be exponential and with the same PL lifetime for different samples.[3]

E. SIMS analysis

We conducted SIMS analysis for selected samples. The results for hydrogen in Am-*n*-GaN and Am-n^+-GaN are summarized in Fig. 10. After annealing at 1050 °C in ambient pressure N_2 or at 1000 °C under ultra-high N_2 pressure, the concentration of H remained nearly unchanged (1.5×10^{19} cm^{-3} for Am-*n*-GaN and 3×10^{19} cm^{-3} for Am-*n*+-GaN). At 1400 °C under UHPA, it decreased by at least an order of magnitude (the detection limit for H is ~10^{18} cm^{-3}). The stability of H in ammonothermal GaN up to 1000 °C contrasts with its behavior in high-resistivity undoped GaN grown by metalorganic chemical vapor deposition, where hydrogen out-diffuses from samples at $T_{ann} < 800$ °C.[25,28] The oxygen concentration is 1×10^{18} cm^{-3} in Am-*n*-GaN and 1×10^{19} cm^{-3} in Am-n^+-GaN. Annealing up to 1400 °C under UHPA did not cause any significant change in oxygen.

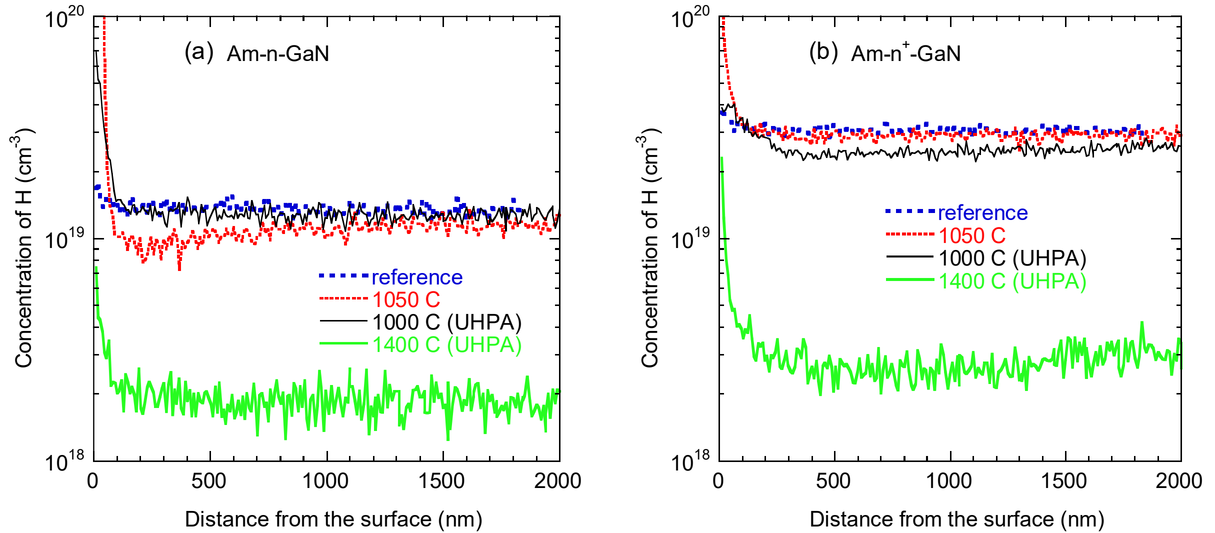

Fig. 10. (Color online) The SIMS profiles of the hydrogen impurity before thermal annealing, after annealing in atmospheric pressure N_2 at 1050 °C and annealing with UHPA method at 1000 and 1400 °C. (a) Am-*n*-GaN, (b) Am-n^+-GaN.

V. DISCUSSION

A. Concentrations of defects revealed by photoluminescence

In general, PL intensity is not necessarily proportional to the concentrations of defects, and a careful analysis of PL data is needed.[3] However, the situation is favorable for studied ammonothermal GaN samples, which are conductive *n*-type even at low temperatures. Samples Am-n^+-GaN are degenerate, with the concentrations of free electrons (n_0) of about 10^{19} cm^{-3}, independent of temperature. By analyzing PL decays of the UVL and BL1 bands in Am-*n*-GaN samples, we concluded that $n_0 \approx 5\times10^{17}$ cm^3 in the Am-*n*-GaN samples for temperatures between 20 and 100 K; i.e., they also behave as degenerate semiconductors.[11] For such semiconductors, the low-temperature defect-related PL intensity is proportional to the defect concentration N_i and its hole-capture coefficient C_{pi}.[3] The hole-capture coefficients for major acceptors contributing to PL in *n*-type GaN are high because of the attractive character and a negligible capture barrier (10^{-6}, 5×10^{-7}, and 4×10^{-7} cm^3/s for the Mg_{Ga}, Zn_{Ga}, and C_N responsible for the UVL, BL1, and YL1 bands, respectively).[3]

1. Rate equations model

The rate equation for free holes with the concentration *p* created in a degenerate *n*-type semiconductor by above-bandgap excitation under steady-state conditions at low temperatures can be written as [22,29]

$$G = \sum_i C_{pi} N_i p \,, \tag{3}$$

where *G* is the electron-hole generation rate, and all recombination channels are included in the sum. We will define i = 0, 1, 2, 3, 4, and 5 for the NBE, UVL, BL1, YL2, OL3, and RL4 bands,

respectively, and $i = 6$ for the nonradiative (N/R) channel. For the NBE emission, $N_i = n_0$ and $C_{pi} = B$, where B is the radiative recombination coefficient.[30] It follows from Eq. (3) that the quantum efficiency of each recombination channel is

$$\eta_i = \frac{C_{pi} N_i}{\sum_j C_{pj} N_j}. \tag{4}$$

The concentrations of defects N_i and their dependences on T_{ann} can be estimated by using Eq. (4) and the $\eta_i(T_{ann})$ dependences found experimentally (Fig. 7). The following assumptions are made: a) the coefficients C_{pi} are not affected by T_{ann} if the defects do not change their composition or structure; b) the N_i for the UVL, BL1, and NBE bands are independent of T_{ann} because the impurities are immobile at studied annealing temperatures and n_0 does not change; c) the concentrations of the complexes containing the V_{Ga} and H_i components may increase or decrease by orders of magnitude due to formation or dissociation of complexes because both V_{Ga} and H_i are expected to be mobile in GaN, at least at $T_{ann} > 500$ °C (Sec. VB). The $C_{pi}N_i$ (T_{ann}) dependences obtained from Eq. (4) by using the data from Fig. 7 are shown in Fig. 11.

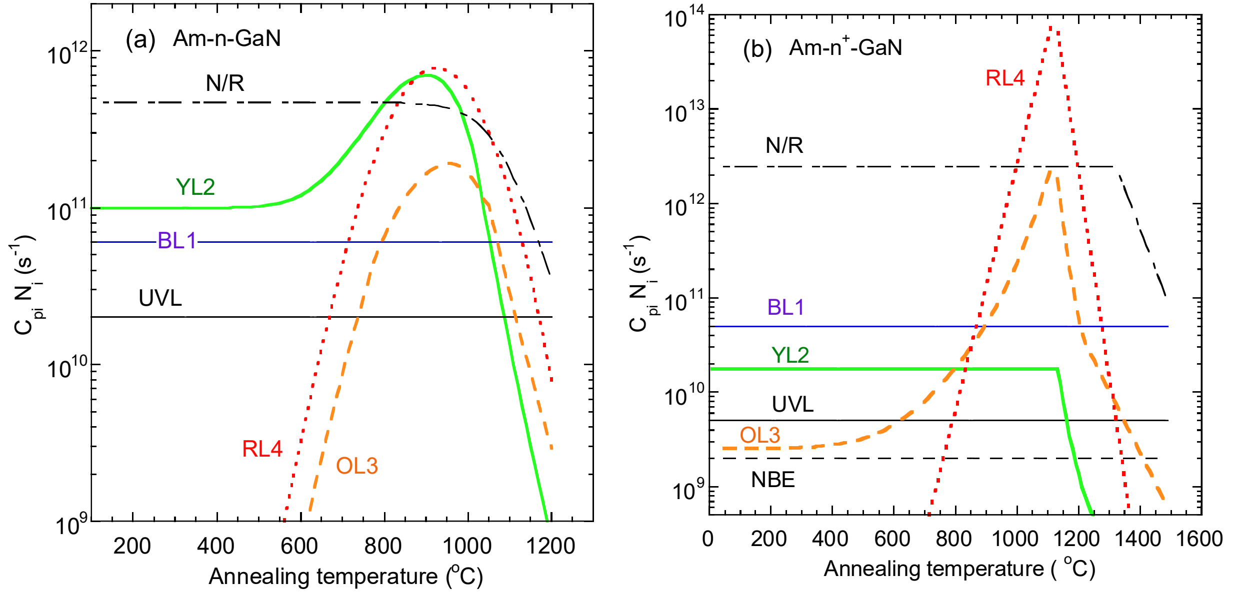

Fig. 11. (Color online) The simulated dependences of the terms N_iC_{pi} on T_{ann} for the recombination channels. (a) Am-n-GaN, (b) Am-n^+-GaN. These $N_iC_{pi}(T_{\text{ann}})$ dependences substituted into Eq. (4) were used to plot the calculated $\eta_i(T_{\text{ann}})$ dependences in Fig. 7.

The terms $C_{pi}N_i$ for the UVL and BL1 and the η_i values for these bands at low T_{ann} serve as the reference in finding $C_{pi}N_i$ for other defects. We have set $C_{p1}N_1 = 2\times10^{10}$ s^{-1} (Am-n-GaN) and $C_{p1}N_1 = 5\times10^9$ s^{-1} (Am-n^+-GaN) for the UVL band, and $C_{p2}N_2 = 6\times10^{10}$ s^{-1} (Am-n-GaN) and $C_{p2}N_2 = 5\times10^{10}$ s^{-1} (Am-n^+-GaN) for the BL1 band (Fig. 11). The relative values of these $C_{pi}N_i$ are proportional to the quantum efficiencies (or integrated PL intensities) of the UVL and BL1 bands in the two types of the Am-GaN samples. The absolute values of these $C_{pi}N_i$ are consistent with typical concentrations of Mg and Zn impurities in our GaN samples ($N_1 = 1.5\times10^{16}$ cm^{-3} and $N_2 = 6\times10^{16}$ cm^{-3} in Am-n-GaN, and $N_1 = 4\times10^{15}$ cm^{-3} and $N_2 = 5\times10^{16}$ cm^{-3} in Am-n^+-GaN)[1] and known hole-capture coefficients for the UVL and BL1 bands ($C_{p1} = 10^{-6}$ cm^3/s and $C_{p2} = 5\times10^{-7}$ cm^3/s).[3] The term $C_{pi}N_i$ for the YL2 band in the limit of low T_{ann} is set to $C_{p3}N_3 = 10^{11}$ s^{-1} (Am-n-GaN) and $C_{p3}N_3 = 1.8\times10^{10}$ s^{-1} (Am-n^+-GaN) according to the relative integrated PL intensity of this band.

2. Am-n-GaN samples

First, we will analyze the dependences of $C_{pi}N_i$ on T_{ann} for Am-*n*-GaN samples (Fig. 11a). With increasing T_{ann} from 600 to 800 °C, the YL2, OL3, and RL4 intensities increase, whereas the BL1, UVL, and NBE intensities decrease (Fig. 7a, the NBE data with $C_{pi}N_i < 10^9$ s^{-1} are not shown). Since the terms N_iC_{pi} with i = 0, 1, 2, and 6 are constant, we conclude that the *concentrations* of the YL2, OL3, and RL4 defects (i = 3, 4, and 5) increase between 600 and 900 °C. The increase in N_iC_{pi} occurs due to the increase in N_i because C_{pi} is independent of T_{ann}. The total efficiency of the last three channels approaches unity at T_{ann} = 900-1000 °C. As a result of a competition between the recombination channels, the quantum efficiencies of the first four channels (i = 0, 1, 2, and 6) decrease at these temperatures.

At higher annealing temperatures, the quantum efficiencies of channels with i = 0, 1, and 2 increase (Fig. 7a). At T_{ann} = 1100 °C, these efficiencies exceed the values in the limit of low T_{ann}, and the BL1 and UVL bands become the strongest PL bands at T_{ann} = 1400 °C, with the total quantum efficiency close to one. The rise of the NBE, UVL, and BL1 bands with T_{ann} above 1000 °C and the simultaneous decrease of the YL2, OL3, and RL4 intensities indicate that the concentrations of defects responsible for the latter three PL bands decrease. Moreover, the efficiency of the nonradiative channel must decrease above 1000-1100 °C. This assumption is necessary to explain the increase in the NBE, UVL, and BL1 efficiencies compared to their values at T_{ann} < 600 °C.

From the obtained values of N_iC_{pi} for the YL2, OL3, and RL4 bands, we can estimate the concentrations of the related defects in Am-*n*-GaN. At T_{ann} ≈ 900-1000 °C, $N_i \approx 6\times10^{17}$, 2×10^{17}, and 7×10^{17} cm^{-3} for the YL2, OL3, and RL4 defects, respectively, if $C_{pi} = 10^{-6}$ cm^3/s. An important

conclusion from the above analysis is that the concentrations of the YL2, OL3, and RL4 defects increase from 600 to 800 °C, approximately with the activation energy of 2-3 eV. At $T_{ann} > 1000$ °C, the concentrations of these defects decrease with the activation energy of about 3 eV. In addition, the concentration of unknown nonradiative defect with a high quantum efficiency at $T_{ann} < 600$ °C ($\eta_6 \approx 0.7$) also decreases with about the same activation energy at $T_{ann} > 1000$ °C. The concentration of this nonradiative defect before the annealing is 5×10^{17} cm^{-3} if $C_{pi} = 10^{-6}$ cm^3/s.

3. Am-n⁺-GaN samples

A similar analysis was conducted for the Am-n^+-GaN samples (Figs. 7b and 11b). As in the Am-n-GaN case, the rise of the RL4 band at $T_{ann} > 800$ °C causes a significant decrease in the NBE, UVL, and BL1 intensities (Figs. 5b, 6b, 7b). At $T_{ann} \approx 1100$ °C, the quantum efficiency of the RL4 band approaches unity, and those of the NBE, UVL, and BL1 decrease to a minimum. This is a result of the competition for photogenerated holes between recombination channels, according to which the quantum efficiencies of all recombination channels decrease by a factor of $R = (1-\eta)^{-1}$ where η is the quantum efficiency of the channel with the efficiency approaching unity.[3,29] From the drop in the NBE, UVL, and BL1 intensities by a factor of 30-50, we can estimate that $\eta \approx 0.98$ for the RL4 band at this annealing temperature.

At higher annealing temperatures, the quantum efficiencies of the OL3 and RL4 bands decrease, and those of the NBE, UVL, and BL1 bands significantly increase. Qualitatively, the behavior of all the recombination channels with annealing in the Am-n^+-GaN samples is the same as in the Am-n-GaN samples, while the temperatures at which the concentrations of the defects increase and then decrease are not the same. The maximum concentrations of the defects in Am-n^+-GaN are 2×10^{16} cm^{-3} (YL2), 2×10^{18} cm^{-3} (OL3), and 8×10^{19} cm^{-3} (RL4) at $T_{ann} \approx 1100$ °C,

while the concentration of nonradiative defects before the annealing is 2.5×10^{18} cm^{-3} if $C_{pi} = 10^{-6}$ cm^3/s for the YL2, OL3, RL4 bands, and the nonradiative defect.

4. The NBE emission

The NBE emission is strong in the Am-n^+-GaN because of the high n_0 in these samples ($n_0 = 10^{19}$ cm^{-3}). The $C_{pi}N_i$ term for this band, obtained from the relative integrated PL intensities in the reference sample and at low T_{ann}, is equal to $Bn_0 = 2\times10^9$ s^{-1} (Fig. 11b). The value of $B = 2\times10^{-10}$ cm^3/s at $T = 18$ K agrees with the predictions for the radiative recombination coefficient in GaN.[30] The temperature dependence of the NBE quantum efficiency on T_{ann} (shown in Fig. 7b with the × symbols) confirms the estimates made in Sec. VA3. In particular, the η_i for the NBE drops by $R = 40$ with increasing T_{ann} from 800 to 1100 °C, which agrees with $\eta_i = 0.98$ for the RL4 band at $T_{\text{ann}} \approx 1100$ °C. At higher annealing temperatures, the η_i for the NBE increases by a factor of 10^3 and becomes 20 times stronger than in the reference sample or at $T_{\text{ann}} < 600$ °C. This indicates that the efficiency of the nonradiative recombination decreased by a factor of 20 at $T_{\text{ann}} = 1400$ °C. For the Am-n-GaN samples, the parameters $B = 2\times10^{-10}$ cm^3/s and $n_0 = 10^{18}$ cm^{-3} are consistent with the observed NBE quantum efficiency ($\eta_0 = 5\times10^{-4}$ at $T_{\text{ann}} < 600$ °C). The efficiency drops to 2×10^{-5} at $T_{\text{ann}} = 800$-1000 °C, and it increases by more than two orders of magnitude with increasing T_{ann} from 1000 to 1400 °C.

5. A simple method

The concentration of defects responsible for the YL2, OL3, and RL4 bands and unknown nonradiative defects were estimated above by fitting the dependences shown in Fig. 7, where the accuracy of the absolute quantum efficiencies of PL bands may be questioned. However, the validity of these estimates can be demonstrated in a simple way, which does not require finding the absolute internal quantum efficiency. Indeed, it follows from Eq. (4) that

$$\frac{\eta_i}{\eta_j} = \frac{I_i^{PL}}{I_j^{PL}} = \frac{C_{pi}N_i}{C_{pj}N_j}, \quad (5)$$

where I^{PL} is the integrated PL intensity of a particular PL band. Then, by finding the I_i^{PL}/ I_j^{PL} ratio from the experiment and using the $C_{pj}N_j$ for the NBE, UVL, and BL1 bands, we can find the $C_{pi}N_i$ for a PL band from an unknown defect. For example, at $T_{\rm ann}$ = 1100 °C (the PL spectrum is shown in Fig. 5b), the integrated PL intensity of the RL4 band is higher than those of the NBE, UVL, and BL1 bands by 5×10^4, 2.5×10^4, and 1.5×10^3, respectively. By taking the typical values of $N_0 = n_0 = 10^{19}$ cm^{-3}, $N_1 = N_{\rm Mg} = 4\times10^{15}$ cm^{-3}, and $N_2 = N_{\rm Zn} = 5\times10^{16}$ cm^{-3} for our Am-n^+-GaN samples,[1] and $C_{p0} = B = 2\times10^{-10}$ cm^3/s, $C_{p1} = 1\times10^{-6}$ cm^3/s, and $C_{p2} = 5\times10^{-7}$ cm^3/s for related PL bands, we obtain $C_{pi}N_i = 1\times10^{14}$, 1×10^{14}, and 4×10^{13} s^{-1}, which is close to the value of 8×10^{13} s^{-1} found in Sec. VA3. Then, $N_i = 8\times10^{19}$ cm^{-3} in assumption that $C_{pi} = 1\times10^{-6}$ cm^3/s. The N_i is even higher if the C_{pi} is smaller. It is unlikely that the C_{pi} is larger than 10^{-6} cm^3/s, especially if the RL4 band is caused by a donor.[3]

B. Mobility of species in ammonothermal GaN

In ammonothermal n-type GaN, we observed PL from three defects, the concentration of which changed significantly with annealing temperature. This behavior indicates that the defects are related to a volatile component that may bind to or dissociate from the defect due to annealing. The only species in the studied GaN that are expected to be mobile at $T_{\rm ann} < 1000$ °C are hydrogen and $V_{\rm Ga}$.

It is well known that hydrogen is mobile in high-resistivity or p-type GaN at $T_{\rm ann} > 500$ °C and can be removed from the sample after annealing in N_2 at 900-1000 °C.[25,28,31,32,33,34] However, in agreement with our SIMS results (Sec. IVE), no diffusion of hydrogen or its release from the

sample is observed up to 1000 °C for conductive *n*-type GaN.[35] Furthermore, after annealing in H_2+NH_3 atmosphere at 1020 °C hydrogen diffuses into the *p*-type layer but does not enter into the *n*-type layer.[35] These phenomena are explained by the fact that H_i is negatively charged in *n*-type GaN and positively charged in *p*-type or high-resistivity GaN when the Fermi level is lower than ~3 eV above the VBM.[25] According to first-principles calculations, mobility of the H_i^+ is much higher than that of the H_i^-.[34,36,37] We may also expect that removing the hydrogen out of the degenerate *n*-type GaN is also more difficult than from *p*-type or high-resistivity GaN. However, the annealing-induced dissociation of complexes is possible even if hydrogen does not diffuse out of the sample.

On the other hand, the V_{Ga} is expected to be mobile at relatively low temperatures. Saarinen *et al*.[38] concluded that the V_{Ga} defects created in bulk GaN by 2-MeV electron irradiation become mobile at $T_{ann} \approx 300$ °C. They estimated the migration barrier for the V_{Ga} as ~1.5 eV. From first-principles calculations, the migration barrier for the V_{Ga}^{3-} in GaN is 1.9 eV.[39] Furthermore, Horibuchi *et al*.[40] observed the formation of helical dislocations after annealing ammonothermal GaN substrate at 1100 °C. They proposed that mobile vacancies are condensed at screw dislocations and deform them in a specific way. Vacancies may also aggregate to form structural defects such as voids.[40] Thus, at least for $T_{ann} > 1000$ °C, we expect the dissociation of the V_{Ga}-containing complexes, diffusion of the vacancies, and their segregation at structural defects or removal from the sample.

C. Identification of PL bands

The new PL bands' shapes, positions, and properties are different from those observed for PL bands in GaN grown by other methods.[3] In particular, the C_N-related YL1 band has a maximum at

2.15 eV, ZPL at 2.59 eV, and is quenched in n-type GaN at much higher temperatures than the YL2 band. The predicted in Sec. III ZPL and PL band maximum for transitions via the 0/+ level of the V_{Ga}-$3H_i$ complex (E_0 = 2.78 eV and $\hbar$ = 2.13 eV) are close to the parameters of the YL2 band (E_0 = 2.9 eV and $\hbar$ = 2.3 eV). These complexes may be abundant in ammonothermal GaN. It is possible that some other donor-like complexes, such as V_{Ga}-O_N-$2H_i$ and V_{Ga}-$2O_N$-H_i (Sec. III), also contribute to the YL2 band. If the PL lifetimes associated with these complexes are slightly different from that of the YL2 and their positions and shapes are close, their presence would explain large shifts of the YL2 band and nonexponential decay even at room temperature.[11] The rise in the concentration of the YL2 defect at T_{ann} = 600-800 °C (Fig. 11a) can be explained by the dissociation of the V_{Ga}-$4H_i$ complexes and the formation of the V_{Ga}-$3H_i$ defects.

Similarly, ZPL and PL band maximum for transitions via the 0/+ level of the V_{Ga}-$3O_N$ complex (E_0 = 2.28 eV and $\hbar$ = 1.67 eV) are close to the parameters of the RL4 band ($E_0 \approx$ 2.3 eV and $\hbar$ = 1.6-1.7 eV). The appearance of the RL4 band at T_{ann} > 600 °C and its abundance at T_{ann} = 1000-1100 °C can be explained by dissociation of the V_{Ga}-$3O_N$-H_i complexes and formation of the V_{Ga}-$3O_N$ defects. The experimental data indicate that the RL4 band is caused by electron transitions from the conduction band to a defect level at ~1.2 eV above the valence band. The PL is not caused by internal transitions from an excited state to the ground state of the defect because the PL decay is nonexponential at low temperatures, and the effective PL lifetime is sample-dependent (Sec. IVD). The quantum efficiency of the RL4 band is close to unity at T_{ann} = 1000-1100 °C. The concentration of the related defect can reach 10^{18} cm^{-3} in Am-n-GaN and 10^{20} cm^{-3} in Am-n^+-GaN (Sec. VB). The extremely high quantum efficiency of the RL4 band in Am-n^+-

GaN also sets a lower limit to the hole-capture coefficient of the related defect – close to 10^{-6} cm^3/s. At $T_{ann} > 1000$ °C, the complex dissociates, and the RL4 intensity decreases.

The origin of the weaker OL3 band is unknown. Two possible candidates are the V_{Ga}-$2O_N$-H_i, and V_{Ga}-O_N-$2H_i$ complexes with predicted $\hbar$ = 1.79 and 1.92 eV, respectively (Sec. III). In any case, the defect is a complex, the composition of which can be changed by annealing.

At $T_{ann} > 1000$ °C, the dissociation of several V_{Ga}-containing complexes begins. As a result, the concentration of defects responsible for the RL4, YL2, and OL3 bands decreases with the activation energy of 2-4 eV. Due to hydrogen removal, the acceptor-like complexes $V_{Ga}O_N$, V_{Ga}-$2O_N$, $V_{Ga}H_i$, V_{Ga}-$2H_i$, and $V_{Ga}O_NH_i$, are expected to form and eventually dissociate. We suggest (Sec. III) that all these defects are nonradiative recombination centers. Interestingly, our PL results show (yet indirectly) that a nonradiative defect with high recombination efficiency dissociates at $T_{ann} > 1100$ °C (Fig. 11). It could be one of the V_{Ga} complexes behaving as a nonradiative recombination center.

The effect of annealing on PL from ammonothermal GaN was studied by other researchers. Uedono *et al.*[6] observed that the intensity of a yellow band with a maximum at ~2.2 eV slightly increased (relative to the NBE intensity) after annealing of acidic ammonothermal GaN in N_2 atmosphere at 1000 °C for 24 hours. Iso *et al.*[41] studied *c*- and *m*-plane GaN substrates also grown by acidic ammonia technology. After annealing at 1150 °C for 30 min, the yellow band with a maximum at 2.2 eV disappeared in *m*-plane GaN substrate but remained unchanged in *c*-plane GaN substrate. It is difficult to compare the results in these works with ours because the defects in samples grown by different research groups may not be the same. Moreover, shapes and positions

of broad PL bands are sensitive to corrections for the spectral response of the measurement system,[3] which is often ignored.[6]

VI. CONCLUSION

PL spectrum from GaN grown by ammonothermal method contains the YL2 band with a maximum at 2.3 eV. We attribute this band to electron transitions from the conduction band to the 0/+ level of the V_{Ga}-$3H_i$ complex. According to our first-principles calculations and SIMS analysis, this defect and other complexes containing the V_{Ga}, H_i, and O_N are abundant in ammonothermal GaN. However, most of these complexes do not contribute to PL in the visible part of the spectrum. When the samples are annealed at T_{ann} > 600 °C, the dissociation of the complexes and the formation of new complexes occur. The concentration of new complexes dramatically increases with annealing temperature, which causes two bright PL bands: the OL3 at 2.1 eV and the RL4 band at 1.6-1.7 eV. We propose that the dissociation of the V_{Ga}-$3O_N$-H_i complex leads to the creation of the V_{Ga}-$3O_N$ defect. This defect is radiative, and the expected PL band matches the properties of the RL4 band. The quantum efficiency of the RL4 band approaches unity at T_{ann} = 1000-1100 °C, indicating that the related defect has a very high concentration and hole-capture coefficient. At T_{ann} > 1100 °C, the intensities of the YL2, OL3, and RL4 bands decrease, and the intensities of the Mg- and Zn-related UVL and BL1 bands simultaneously increase. Such behavior of PL indicates that the defect complexes responsible for the YL2, OL3, and RL4 dissociate at these temperatures.

Acknowledgments

The work at VCU was supported by the National Science Foundation (grant DMR-1904861). The calculations were performed at the VCU Center for High Performance Computing.

This research was also supported by the Polish National Science Center through project 2020/37/B/ST5/03746, as well as by the TEAM TECH program of the Foundation for Polish Science co-financed by the European Union under the European Regional Development Fund (POIR.04.04.00-00-5CEB/17-00).

Data Availability

The data that support the findings of this study are available from the corresponding author upon reasonable request.

References

[1] M. Zajac, R. Kucharski, K. Grabianska, A. Gwardys-Bak, A. Puchalski, D. Wasik, E. Litwin-Staszewska, R. Piotrzkowski, J. Z. Domagala, and M. Bockowski, "Basic ammonothermal growth of Gallium Nitride – State of the art, challenges, perspectives", Progress in Crystal Growth and Characterization of Materials **64**, 63-74 (2018).

[2] M. A. Reshchikov and H. Morkoç, "Luminescence properties of defects in GaN", J. Appl. Phys. **97**, 061301 (2005).

[3] M. A. Reshchikov, "Measurement and analysis of photoluminescence in GaN", J. Appl. Phys. **129**, 121101 (2021).

[4] F. Tuomisto, J.-M. Mäki, and M. Zając, "Vacancy defects in bulk ammonothermal GaN crystals", J. Crystal Growth **312**, 2620-2623 (2010).

[5] S. Suihkonen, S. Pimputkar, S. Sintonen, and F. Tuomisto, "Defects in single crystalline ammonothermal gallium nitride", Adv. Electron. Mater. **3**, 1600496 (2017).

[6] A. Uedono, Y. Tsukada, Y. Mikawa, T. Mochizuki, H. Fujisawa, H. Ikeda, K. Kurihara, K. Fujito, S. Terada, S. Ishibashi, and S. F. Chichibu, "Vacancies and electron trapping centers in acidic ammonothermal GaN probed by a monoenergetic positron beam", J. Crystal Growth **448**, 117-121 (2016).

[7] F. Tuomisto, T. Kuittinen, M. Zając, R. Doradziński, and D. Wasik, “Vacancy-hydrogen complexes in ammonothermal GaN”, J. Crystal Growth **403**, 114-118 (2014).

[8] S. Suihkonen, S. Pimputkar, J. S. Speck, and S. Nakamura, “Infrared absorption of hydrogen-related defects in ammonothermal GaN”, Appl. Phys. Lett. **108**, 202105 (2016).

[9] W. Jiang, M. Nolan, D. Ehrentraut, and M. P. D’Evelyn, “Electrical and optical properties of gallium vacancy complexes in ammonothermal GaN”, Appl. Phys. Express **10**, 075506 (2017).

[10] J. L. Lyons, A. Alkauskas, A. Janotti, and C. G. Van de Walle, “First-principles theory of acceptors in nitride semiconductors”, Phys. Stat. Sol. B **252**, 900-908 (2015).

[11] M. A. Reshchikov, M. Vorobiov, K. Grabianska, M. Zajac, M. Iwinska, and M. Bockowski, “Defect-related photoluminescence from ammono GaN”, J. Appl. Phys. 129, 095703 (2021).

[12] J. Heyd, G. E. Scuseria, and M. Ernzerhof, “Hybrid functionals based on a screened Coulomb potential”, J. Chem. Phys. **118**, 8207 (2003).

[13] D. O. Demchenko, I. Diallo, and M. A. Reshchikov, “Magnesium acceptor in gallium nitride: II. Koopmans tuned HSE hybrid functional calculations of dual nature and optical properties”, Phys. Rev. B **97**, 205205 (2018).

[14] C. Freysoldt, J. Neugebauer, and C. G. Van de Walle, “Fully *Ab Initio* Finite-Size Corrections for Charged-Defect Supercell Calculations”, Phys. Rev. Lett. **102**, 016402 (2009).

[15] C. Freysoldt, J. Neugebauer, and C. G.Van de Walle, “Electrostatic interactions between charged defects in supercells”, Phys. Stat. Sol. (b) **248**, 1067-1076 (2011).

[16] C. Freysoldt, B. Grabowski, T. Hickel, J. Neugebauer, G. Kresse, A. Janotti, and C. G. Van de Walle, “First-principles calculations for point defects in solids”, Rev. Mod. Phys. **86**, 253-305 (2014).

[17] R. Kucharski, T. Sochacki, B. Lucznik, and M. Bockowski, “Growth of bulk GaN crystals”, J. Appl. Phys. **128**, 050902 (2020).

[18] K. Grabianska, R. Kucharski, A. Puchalski, T. Sochacki, and M. Bockowski, “Recent progress in basic ammonothermal GaN crystal growth”, J. Cryst. Growth **547**, 125804 (2020).

[19] R. Doradzinski, R. Dwilinski, J. Garczynski, L. P. Sierzputowski, and N. D. Y. Kanbara, in *Technology of Gallium Nitride Crystal Growth*, edited by D. Ehrentraut, E. Meissner, and M. Bockowski (Springer-Verlag, Heidelberg, 2010), pp. 137–158.

[20] K. Sierakowski, R. Jakiela, B. Lucznik, P. Kwiatkowski, M. Iwinska, M. Turek, H. Sakurai, T. Kachi, and M. Bockowski, "High Pressure Processing of Ion Implanted GaN - MDPI", Electronics **9**, 1380 (2020)

[21] M. A. Reshchikov, M. Vorobiov, D. O. Demchenko, Ü. Özgür, H. Morkoç, A. Lesnik, M. P. Hoffmann, F. Hörich, A. Dadgar, and A. Strittmatter, "Two charge states of the C_N acceptor in GaN: Evidence from photoluminescence", Phys. Rev. B **98**, 125207 (2018).

[22] M. A. Reshchikov, A. A. Kvasov, M. F. Bishop, T. McMullen, A. Usikov, V. Soukhoveev, and V. A. Dmitriev, "Tunable and abrupt thermal quenching of photoluminescence in high-resistivity Zn-doped GaN", Phys. Rev. B **84**, 075212 (2011).

[23] A. Alkauskas, C. E. Dreyer, J. L. Lyons, and C. G. Van de Walle, "Role of excited states in Shockley-Read-Hall recombination in wide-band-gap semiconductors", Phys. Rev. B **93**, 201304 (2016).

[24] D. O. Demchenko, I. C. Diallo, and M. A. Reshchikov, "Hydrogen-carbon complexes and the blue luminescence band in GaN", J. Appl. Phys. **119**, 035702 (2016).

[25] M. A. Reshchikov, O. Andrieiev, M. Vorobiov, B. McEwen, F. Shahedipour-Sandvik, D. Ye, and D. O. Demchenko, "Stability of the C_NH_i complex and the BL2 luminescence band in GaN", Phys. Stat. Sol. (b) 2100392 (2021).

[26] M. A. Reshchikov, D. O. Demchenko, J. D. McNamara, S. Fernández-Garrido, and R. Calarco, "Green luminescence in Mg-doped GaN", Phys. Rev. B **90**, 035207 (2014).

[27] R. Y. Korotkov, M. A. Reshchikov, and B. W. Wessels, "Acceptors in undoped GaN studied by transient photoluminescence", Physica B **325**, 1-7 (2003).

[28] S. Wu, X. Yang, Q. Zhang, Q. Shang, H. Huang, J. Shen, X. He, F. Xu, X. Wang, W. Ge, and B. Chen, "Direct evidence of hydrogen interaction with carbon: C-H complex in semi-insulating GaN", Appl. Phys. Lett. **116**, 262101 (2020).

[29] M. A. Reshchikov, M. A. Foussekis, J. D. McNamara, A. Behrends, A. Bakin, and A.Waag, "Determination of the absolute internal quantum efficiency of photoluminescence in GaN co-doped with Zn and Si", J. Appl. Phys. **111**, 073106 (2012).

[30] A. Dmitriev and A. Oruzheinikov, "The rate of radiative recombination in the nitride semiconductors and alloys", J. Appl. Phys. **86**, 3241-3246 (1999).

[31] S. Nakamura, T. Mukai, M. Senoh, and N. Iwasa, "Thermal annealing effects on *p*-type Mg-doped GaN films", Jpn. J. Appl. Phys. **31**, Pt. 2, L139-L142 (1992).

[32] W. Götz, N. M. Johnson, J. Walker, D. P. Bour, H. Amano, and I. Akasaki, "Hydrogen passivation of Mg acceptors in GaN grown by metalorganic chemical vapor deposition", Appl. Phys. Lett. **67**, 2666-2668 (1995).

[33] A. Y. Polyakov, N. B. Smirnov, S. J. Pearton, F. Ren, B. Theys, F. Jomard, Z. Teukam, V. A. Dmitriev, A. E. Nikolaev, A. S. Usikov, and I. P. Nikitina, "Fermi level dependence diffusivity in GaN", Appl. Phys. Lett. **79**, 1834-1836 (2001).

[34] S. M. Myers, A. F. Wright, G. A. Petersen, W. R. Wampler, C. H. Seager, M. H. Crawford, and J. Han, "Diffusion, release, uptake of hydrogen in magnesium-doped gallium nitride: Theory and experiment", J. Appl. Phys. **89**, 3195-3202 (2001).

[35] R. Czernecki, E. Grzanka, R. Jakiela, S. Grzanka, C. Skierbiszewski, H. Turski, P. Perlin, T. Suski, K. Donimirski, and M. Leszczynski, "Hydrogen diffusion in GaN:Mg and GaN:Si", J. Alloys and Compounds **747**, 354-358 (2018).

[36] J. Neugebauer and C. G. Van de Walle, "Hydrogen in GaN: Novel Aspects of a Common Impurit", Phys. Rev. Lett. **75**, 4452-4455 (1995).

[37] S. Limpijumnong and C. G. Van de Walle, "Stability, diffusivity, and vibrational properties of monoatomic and molecular hydrogen in wurtzite GaN", Phys. Rev. B **68**, 235203 (2003).

[38] K. Saarinen, T. Suski, I. and D. C. Look, "Thermal stability of isolated and complexed Ga vacancies in GaN bulk crystals", Phys. Rev. B **64**, 233201 (2001).

[39] S. Limpijumnong and C. G. Van de Walle, "Diffusivity of native defects in GaN", Phys. Rev. B **69**, 035207 (2004).

[40] K. Horibuchi, S. Yamaguchi, Y. Kimoto, K. Nishikawa, and T. Kachi, “Formation of helical dislocations in ammonothermal GaN substrate by heat treatment”, Semicond. Sci. Technol. **31**, 034002 (2016).

[41] K. Iso, Y. Mikawa, H. Ikeda, K. Hotta, T. Mochizuki, and S. Izumisawa, Thermal annealing effects on SCAAT™ substrate grown toward the *c*- and *m*-directions”, Appl. Phys. Express **12**, 125502 (2019).